

Available online at www.sciencedirect.com

ScienceDirect

www.elsevier.com/locate/jmbbm

Research Paper

Incipient plasticity in 4H-SiC during quasistatic nanoindentation [☆]



Saurav Goel^{a,b,*}, Jiwang Yan^b, Xichun Luo^c, Anupam Agrawal^d

^aSchool of Mechanical and Aerospace Engineering, Queen's University, Belfast BT95AH, UK

^bDepartment of Mechanical Engineering, Keio University, Yokohama 223-8522, Japan

^cDepartment of Design, Manufacture and Engineering Management, University of Strathclyde, Glasgow G11XQ, UK

^dDepartment of Business Administration, University of Illinois at Urbana Champaign, 61820, USA

ARTICLE INFO

Article history:

Received 11 September 2013

Received in revised form

2 December 2013

Accepted 4 December 2013

Available online 12 December 2013

Keywords:

SiC

Nanoindentation

Plasticity

Elastic response

ABSTRACT

Silicon carbide (SiC) is an important orthopedic material due to its inert nature and superior mechanical and tribological properties. Some of the potential applications of silicon carbide include coating for stents to enhance hemocompatibility, coating for prosthetic-bearing surfaces and uncemented joint prosthetics. This study is the first to explore nanomechanical response of single crystal 4H-SiC through quasistatic nanoindentation. Displacement controlled quasistatic nanoindentation experiments were performed on a single crystal 4H-SiC specimen using a blunt Berkovich indenter (300 nm tip radius) at extremely fine indentation depths of 5 nm, 10 nm, 12 nm, 25 nm, 30 nm and 50 nm. Load–displacement curve obtained from the indentation experiments showed yielding or incipient plasticity in 4H-SiC typically at a shear stress of about 21 GPa (~an indentation depth of 33.8 nm) through a pop-in event. An interesting observation was that the residual depth of indent showed three distinct patterns: (i) positive depth hysteresis above 33 nm, (ii) no depth hysteresis at 12 nm, and (iii) negative depth hysteresis below 12 nm. This contrasting depth hysteresis phenomenon is hypothesized to originate due to the existence of compressive residual stresses (upto 143 MPa) induced in the specimen by the polishing process prior to the nanoindentation.

Crown Copyright © 2013 Published by Elsevier Ltd. All rights reserved.

1. Introduction

Silicon carbide (SiC) is an extremely hard and brittle non-oxide ceramic material. It has been demonstrated that, due to its superior properties, such as chemical inertness, high thermal conductivity, high carrier saturation velocity, high specific stiffness (E/ρ) and high-temperature resistance, SiC is an appropriate choice to replace silicon for advanced ultra precision engineering

applications especially in the electronic industry (Neudeck and Technology, 2000). SiC is also recognized as a potential candidate for quantum computing applications as a substitute for diamond (Dzurak, 2011), in space-based laser mirrors (Shore et al., 2010) and for the development of the thermal protection system (TPS) materials for defense applications (Newsome et al., 2012). Demand of SiC is growing further in weapons, aerospace, microelectronic and bio-medical applications as well as in

[☆]This paper was presented at the Fifth International Conference on the Mechanics of Biomaterials and Tissues (ICMOBT5).

*Corresponding author at: School of Mechanical and Aerospace Engineering, Queen's University, Belfast BT95AH, UK.

Tel.: +44 028 9097 5625; fax: +44 028 9097 4148.

E-mail addresses: s.goel@qub.ac.uk, sgoel.diamond@gmail.com (S. Goel).

“big-science” programmes such as the European Extremely Large Telescope (E-ELT), the Atacama Large Millimeter/submillimeter Array (ALMA) and next generation extreme ultraviolet (EUV) lithography steppers.

SiC is also finding amazing applications in bio-medical sector especially as being a semi-conductor material because of being more bio-compatible over silicon (Coletti et al., 2007). Traditional orthopedic materials such as cobalt chrome (CoCr), stainless steel and titanium on account of being low wear and oxidation resistant, succumb to bone loss which causes implant loosening resulting in a reactive implant surface while SiC is capable of permanently integrating into the new bone growth on account of low wear debris and metallosis and is thus very effective as coating for stents to enhance hemocompatibility and as a coating for prosthetic-bearing surfaces and uncemented joint prosthetics (Li et al., 2005). Nanocrystalline silicon carbide (SiC) is therefore known to carry the potential to become an important and an interface biomaterial which will connect the three disparate disciplines of electronics, material science and biological world (Coletti et al., 2006). Field results of Kalnins et al. (2002) applied directly on various patients provide further support for the above arguments: they found that amorphous silicon carbide stents are more effective than stainless steel in reducing the early and late coronary events.

Mechanical processing of SiC in particular is a daunting task at the moment owing primarily to the following unique characteristics of SiC (Inasaki, 1987; Komanduri, 1996):

1. SiC exhibits low thermal coefficient and high thermal conductivity. This is because of the higher proportion of covalent bonding compared to ionic bonding in SiC (9:1) with the nature of bonding dependent on the Goldschmidt number. The higher proportion of covalent bonding in SiC makes it relatively insensitive to elevated temperature deformation and thus SiC cannot easily be deformed even at elevated temperatures.
2. The ratio of Young's modulus and Vickers hardness in SiC is only about 20 which signify that SiC is highly brittle. This is in contrast to soft ductile materials where this ratio could be as high as 250.
3. The ratio of tensile strength to shear strength in SiC is extremely low (~ 1.5) in contrast to soft ductile metals where this ratio is as high as 10, making them easier to deform through plastic deformation rather than brittle fracture.
4. Low density and low mobility of dislocations leads to high hardness in SiC, while low surface energy due to small density of electrons and high Young's modulus are the reasons of extreme brittleness in SiC. Owing to low surface energy and high Young's modulus, SiC exhibits low fracture toughness and thus poor machinability.
5. To induce the plastic deformation in a ceramic material such as SiC, it requires five independent slip systems to meet the von Mises criterion otherwise twinning or fracture prevails.

Furthermore, SiC exhibits one-dimensional polymorphism: all polytypes have the same tetrahedral arrangement of Si and C atoms but different stacking sequences. It is due to this reason that almost 250 polytypes of silicon carbide (SiC) have been recognized to date (Perrone, 2007). Across all

other polytypes, two major polymorphs are α -SiC and β -SiC with hexagonal and zinc-blende lattice structures, respectively. The main engineering properties of β -SiC (3C-SiC) and α -SiC (6H-SiC and 4H-SiC) have already been summarized elsewhere (Luo et al., 2012).

In the past, experimental trials have been reported on polycrystalline 3C-SiC (CVD-SiC) (Ravindra et al., 2013; Zhao et al., 2011), single crystal 6H-SiC (Patten et al., 2005; Levitas et al., 2012; Goel et al., 2013), polycrystalline 6H-SiC (reaction bonded SiC) (Yan et al., 2009) and single crystal 4H-SiC (Shayan et al., 2009; Ravindra and J.A., 2007). These studies were focused on exploring the ductile-regime machining of SiC and have shown that single crystal 6H-SiC exhibits a ductile to brittle transition (DBT) depth of only 70 nm (Patten et al., 2007) whereas DBT depth in CVD 3C-SiC (polycrystalline) was found to be 550 nm (Bhattacharya et al., 2006). Compared to these two types of SiC, single crystal 4H-SiC showed a much higher DBT depth of up to 820 nm (Ravindra and J.A., 2007). Besides offering a larger DBT depth, 4H-SiC also offers the best machined surface and sub-surface integrity (Luo et al., 2012) across all other major polytypes of SiC which means that it is possible to obtain higher manufacturing productivity for single crystal 4H-SiC. Hence, an investigation on the nanomechanical response of 4H-SiC is scientifically important at this point of time in order to aid cost effective manufacturing of 4H-SiC. State-of-the-art veritable resolution instruments using *in-situ* and *ex-situ* imaging, quasistatic nanoindentation, acoustic emission detection, and high-temperature testing are providing newer insights into nanoscale mechanics of materials. Quasistatic nanoindentation in particular permits systematic examination to enable better understanding of deformation mechanisms, evaluation of mechanical properties, and aspects of plasticity of brittle materials such as SiC. Furthermore, the onset of plastic deformation in a specimen can be studied from such a test merely by a careful assessment of the Load-displacement ($P-h$) profile. In particular, although pop-in event in the $P-h$ curve may arise due to several reasons depending on the type of specimen e.g. discrete strain accommodation mechanism in metals, formation of cracks in brittle materials or formation of shear bands in metallic glasses (Schuh and Lund, 2004), but the first pop-in event in this study was observed to be associated with the elastic-plastic transition, signifying plastic deformation of the material.

Fig. 1 shows schematically how brittle materials behave differently from ductile materials when they are indented either by a large tipped radii or a small tipped radii indenter. It shows that ductile materials show plastic deformation as the dominant mode of deformation whereas the response of brittle materials is dependent on both the tip radii of the indenter and the magnitude of the load (force applied to the indenter). When brittle materials are indented with a sharp tip, they show plastic deformation at sufficiently low indentation loads, beyond which median and lateral cracks appear (Chen et al., 2005; Ravindra, 2011). The qualitative identification of the elastic-plastic response of brittle materials during their nanoindentation reveal that almost any material, including super-hard substances like diamond and SiC, can be deformed plastically even at low temperatures (Niihara, 1979) under the influence of large hydrostatic stresses. With

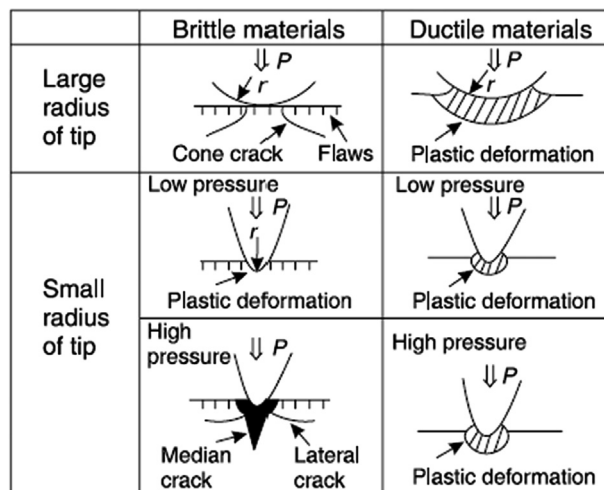


Fig. 1 – Differences in the response of ductile and brittle materials during nanoindentation (Venkatesh and Izman, 2007).

smaller indentation depths, the size of the resulting critical stress field is small enough to avoid cleavage initiated at the defects but, with larger indentation depths, the larger critical stress field allows for sufficient nuclei for crack propagation, which initiate from defects within the material. These factors motivated the current study, wherein quasistatic nanoindentation experiments were conducted on 4H-SiC to study the incipient plasticity from the force–displacement (P – h) curve.

2. Experimental details

The nanoindentation tests were performed on a TI 900 Hysitron TriboIndenter which takes advantage of an acoustic and thermal enclosure that enables capturing precise and sensitive readings (Probe Selection Guide — Hysitron Triboindenter Manual and Incorporated, 2007). Also, its patented capacitive transducer provides superior sensitivity and stability over other similar instruments. The specimen used was a single crystal 4H-SiC wafer having crystal orientation (001), diameter 50 mm and thickness 5 mm which was supplied by PAM-Xiamen Powerway Advanced Material Co. Ltd., China.

The indentation experiments were performed with a three-sided pyramidal Berkovich probe. Of particular relevance in this regard was the nature of the tip apex, which is never atomically sharp and exhibits significant blunting, as measured and verified during the experiments. The method used for the measurement of tip radius involves indenting the tool profile on the copper block. The profile curvature of indentation is copied, fitted to a circle and radius of the circle can be found by simple mathematical analysis (Javvaji, 2008). The measurement revealed the tip radius to be about 300 nm. In the experimental context of the current study, the blunting of the Berkovich tip turned out to be a benefit rather than an experimental difficulty. This is because the blunted geometry of the nanoindenter can often be approximated as spherical (Faisal et al., 2011). With this approximation of the tip geometry, it becomes possible to predict the elastic response using the Hertzian law for mechanical contacts, based on isotropic continuum elasticity. This law predicts a simple power-law form for the elastic portion of the load–displacement

curve, $P \propto h^{3/2}$, (Schuh, 2006) with a proportionality constant that is fully specified by the radius of the blunted indenter tip and the elastic properties of the two contacting materials. The same is evident from the loading curves as shown later.

Based on the above description, a series of displacement controlled quasistatic nanoindentations were performed at different indentation depths. The displacement control feedback system was preferred over load controlled feedback system to limit the total indentation depth so as to avoid specimen effect (Kruzic et al., 2009). The time allowed for reaching maximum displacement in all the cases was 10 s and the indenter was retracted immediately after attaining the peak indentation depth in duration of 10 s. Each test was performed twice (both results were observed to be consistent and hence results for only one set of experiments are presented for brevity). The indents were made following the “quick approach” method. The Quick Approach method moves the indenter tip towards the specimen to sense the exact height of the specimen at a specific point. This move helps in updating the sample safety height with an exact value. Bypassing this step could result in either crashing of the tip into the specimen or would otherwise take several hours to contact the surface. Thus, quick approach method not only helps in ensuring the measurement accuracy at finer depths of indentation, but also ensures that the tip is operated within the “sample safety zones” in that the indenter tip is considered to be safe to avoid any sudden lateral impact load on it. Table 1 shows the various indentation depths used for the experiments. Along with the indentation depth, the table also shows the peak indentation load recorded from the plots obtained from the device and the hysteresis observed in the plots (These are discussed subsequently).

3. Results and discussions

3.1. Depth hysteresis during nanoindentation

The P – h plots for various depths of indentation performed of 4H-SiC are shown in Fig. 2. Fig. 2(a) and (b) shows the

Table 1 – Displacement controlled quasistatic nanoindentation experiments performed on 4H-SiC.

Experiment number	Indenter displacement (h) (nm)	Peak load (P) (μN)	Hysteresis observed
1	5	103	Negative hysteresis
2	10	275	Negative hysteresis
3	12	300	Complete elastic response with no hysteresis
4	25	825	Elastic response with positive hysteresis
5	30	1265	Elastic response with positive hysteresis
6	50	2425	Elastic+Plastic response

P–h plots for the indentation depths of 5 nm and 10 nm respectively.

In both the cases (Fig. 2a and b), a negative depth hysteresis of 12 μN and 20 μN respectively can be observed from these plots. Consequently, at these indentation depths, the Oliver and Pharr method to evaluate the material properties from P–h curve cannot be used. Fig. 3 shows the AFM imaging and the cross section of the area in case where negative depth hysteresis was observed.

In Fig. 3, it may be seen that at sufficiently lower depth of indentation, the surface of the 4H-SiC specimen is projecting upwards (negative depth deviation) after the retraction of the indenter. This is somewhat unusual because extant research on nanoindentation has reported that the unloading curve lags the loading curve and that is why the cross section of the indentation zone shows positive depth deviation. It was not immediately clear as to why this negative depth hysteresis was observed. One thing which may be noted here is that the manufacturer stated that the specimen of 4H-SiC supplied (used in this experimental study) was processed using mechanical polishing process. The presence of residual stresses on the polished surface was thus expected to be present. In order to quantify such residual stresses, Raman spectroscopy was performed. Noticeably, against a regular Raman peak of 776 cm⁻¹ (Feldman et al., 1968) in 4H-SiC, the experiments showed the Raman peak at about 779.29 cm⁻¹. This reveals the extent of compressive residual stresses in the 4H-SiC specimen to be about 143 MPa (compressive).

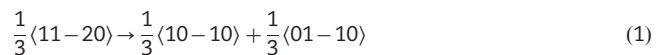
Based on this information, it is proposed that the negative depth hysteresis in the unloading force could be due to the annealing and consequent thermal expansion of the surface layer of the specimen. This could happen due to the local heating (high heat at the interface of the indenter and the specimen due to friction) of the surface layer which helps in relieving the compressive residual stresses that are induced in the specimen due to the polishing process carried out on the specimen prior to the nanoindentation process. While compressive residual stresses get relieved due to annealing, the material expands which might have caused an opposite force on the indenter leading to this negative depth hysteresis. This phenomenon implies and aligns with the concept of backward depth deviation which appears in the form of hogging as has been recently observed in the thin films of Diamond like carbon (DLC) (Faisal et al., 2012) and SiC (Dharma Raju et al., 2003). This implication is also supported from the AFM imaging shown in Fig. 3 which confirms the presence of negative depth deviation.

Fig. 2(c) shows the P–h plot for the indentation made on 4H-SiC specimen at depth of 12 nm. Unlike the indents performed at

depths of 2 nm and 5 nm, no depth hysteresis was observed in these plots. This implies that the material made a complete elastic recovery and unloading curve followed the same trend like that of the loading curve. Fig. 2(d), (e) and (f) shows the P–h plots for the indentation made on 4H-SiC specimen at depths of 25 nm, 30 nm and 50 nm respectively. In these figures, the indentation plot shows a different response of the specimen i.e. the ratio of h_f/h_{max} is less than unity and at an indentation depth of 50 nm a clear positive depth hysteresis is observed from these plots. As explained in the Section 3.2, this positive hysteresis is a result of the incipient plasticity in 4H-SiC. The typical response of the 4H-SiC specimen is schematically presented in Fig. 4, highlighting the behavior of the specimen under different depth of indentations as have been explained below.

3.2. Incipient plasticity in 4H-SiC

Recently, grain boundary (g.b) analysis in conjunction with Large Angle Convergent Beam Electron Diffraction (LACBED) was used to propose that dislocations in 4H-SiC were observed to be in the basal plane with their Burgers vector as 1/3⟨-1-120⟩ (Demenet et al., 2013). Also, perfect dislocations in 4H-SiC were proposed to dissociate into Shockley partials as per the following reaction:



For brittle materials like 4H-SiC, there may be two types of defect nucleations: dislocations or micro-cracks. The dislocations are induced by the onset plasticity, occurring when the maximum shear stress beneath the indenter exceeds the theoretical shear strength of 4H-SiC. The Hertzian theory suggests that the maximum tensile stress is at the edge of the indenter. This stress acts in a radial direction on the surface outside the indenter, and is usually responsible for the cone cracks (Buzio et al., 2003). When the tensile strength does not exceed the value of theoretical cleavage strength or when the maximum shear stress below the indenter tip approaches the theoretical shear strength, then a pop-in event could occur due to the incipient plasticity. Ostensibly, the pop-in event (kink showed in Fig. 2f) arises from the nanomechanical response of the material, possibly due to an activity of defect nucleation or phase transformation underneath the indenter (Schuh, 2006; Chrobak et al., 2013). The parabolic shape of the P–h curve indicates elastic contact while displacement burst plus shallower slope is reminiscent of a combination of elastic and plastic response. Beyond this point, the unloading curve follows the power law curve.

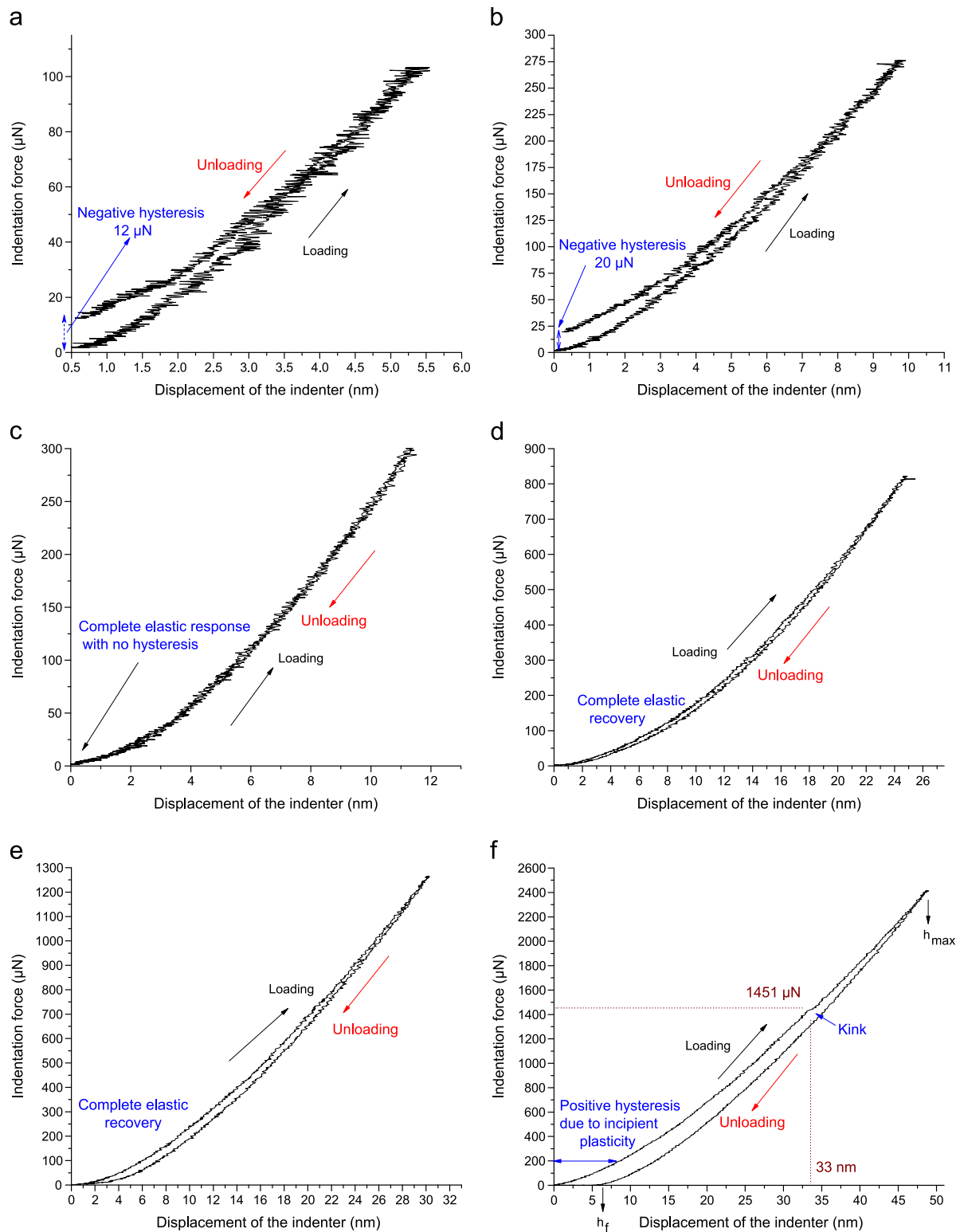


Fig. 2 – P - h plots for indentations made on single crystal 4H-SiC at various depths, (a) Indentation depth 5 nm, (b) Indentation depth 10 nm, (c) Indentation depth 12 nm, (d) Indentation depth 25 nm, (e) Indentation depth 30 nm and (f) Indentation depth 50 nm.

An analytical stress analysis was carried out to find the state of stress underneath the indenter in order to reveal the minutiae of the pop-in event. Before the pop-in event, the P - h curve follows the Hertzian contact theory which could be

expressed using the following equation:

$$P = \frac{4}{3}Er\sqrt{Rh^3} \quad (2)$$

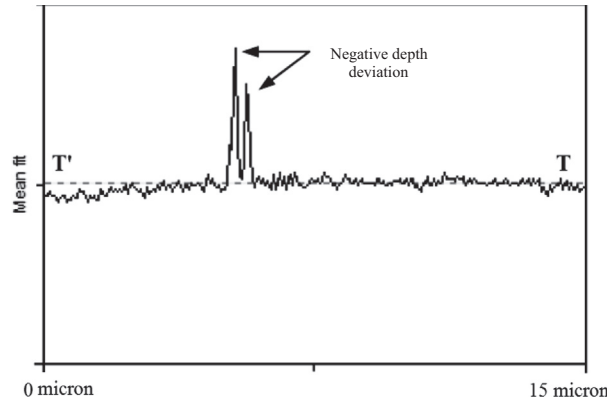


Fig. 3 – AFM imaging and cross section view of the 4H-SiC specimen highlighting the negative depth hysteresis.

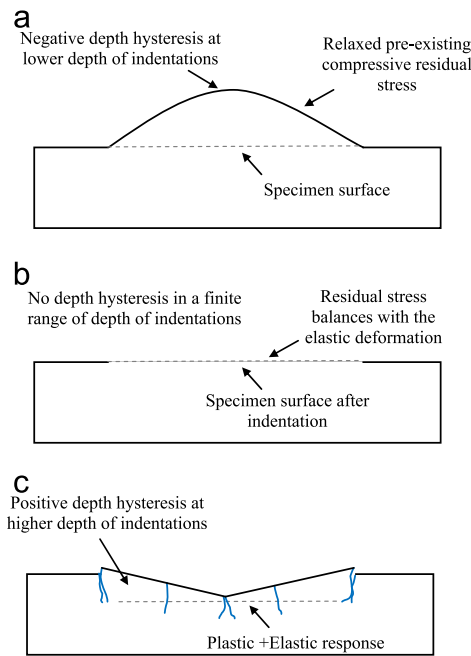


Fig. 4 – Schematic of the depth hysteresis observed during nanoindentation of 4H-SiC, (a) Indentation in 4H-SiC at lower depths of upto 10 nm, (b) Indentation in 4H-SiC at depths 12 nm and (c) Indentation in 4H-SiC at higher depths.

where P is the indentation load, h is the displacement of the indenter, R is the radius of the indenter (300 nm) and E_r is the reduced elastic modulus where E_r can be expressed as:

$$\frac{1}{E_r} = \frac{1-\nu^2}{E} + \frac{1-\nu_i^2}{E_i} \quad (3)$$

In the above expression ν and E are the Poisson's ratio and elastic modulus of 4H-SiC (Luo et al., 2012) respectively while E_i and ν_i are the elastic modulus and Poisson's ratio of the diamond indenter which were considered as 1141 GPa and 0.07 respectively. This gives the value of E_r as 296 GPa for the current combination of diamond and 4H-SiC.

In order to assert if the pop-in event in Fig. 2(f) relates to plastic deformation or crack propagation, an analysis is

presented below. This analysis is based on evaluation of the maximum shear stress and maximum tensile strength underneath the indenter during the process of nanoindentation. The maximum shear stress underneath the indenter can be found out using the following equation (Zhao et al., 2011):

$$\tau = 0.47 \frac{P}{\pi \cdot R \cdot h} \quad (4)$$

This gives an estimate of τ (shear stress) as 21 GPa at an indentation depth of 33 nm at a typical indentation load ($P=1500 \mu\text{N}$) where pop-in event was observed. To compare and correlate this shear stress with plastic deformation, the theoretical shear strength of 4H-SiC was obtained from the following equation (Gouldstone et al., 2000):

$$\text{Shear strength of 4H-SiC} = \frac{G}{2\pi} = \frac{131.4}{2\pi} = 20.9 \text{ GPa} \quad (5)$$

where G is the shear modulus and is experimentally known to be about 131.4 GPa for 4H-SiC.

It can be seen that the shear strength of 4H-SiC (20.9 GPa) corroborates well with the shear stress of 21 GPa estimated to be underneath the indenter during the pop-in event. This seems to suggest an occurrence of plastic deformation in 4H-SiC underneath the indenter. It is to be noted that plastic deformation can be affirmed if another criterion for plastic deformation is fulfilled i.e. the tensile stresses underneath the indenter need to be lower than the cleavage strength of 4H-SiC.

The tensile stresses and cleavage strength of 4H-SiC were obtained using the following equation (Zhao et al., 2011):

$$\sigma_{\max} = \left(\frac{1-2\nu}{2\pi} \right) \left(\frac{4E}{3R} \right)^{2/3} P^{1/3} \quad (6)$$

where σ_{\max} is the tensile strength underneath the indenter, P is the indentation load (1500 μN), ν is the Poisson's ratio (0.23) of 4H-SiC, E is the elastic modulus (347 GPa) (Luo et al., 2012) of 4H-SiC and R is the indenter radius (300 nm).

Substitution of the experimental values in the above equation reveals the magnitude of tensile stress to be about 10.155 GPa underneath the indenter. For fracture or cleavage to dominate over plastic deformation, the cleavage strength of 4H-SiC must be lower than the value of this tensile stress.

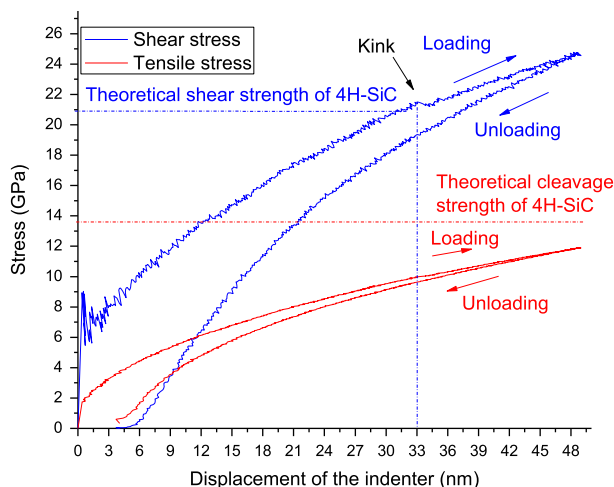


Fig. 5 – Evolution of shear stress and tensile stress underneath the Berkovich indenter (300 nm edge radius) during nanoindentation of nanocrystalline 4H-SiC at indentation depths up to 50 nm

The following equation was used to calculate the cleavage strength of 4H-SiC.

$$\text{Cleavage strength of 4H-SiC} = \frac{1}{2} \sqrt{\frac{E\gamma}{a}} \quad (7)$$

where E is the elastic modulus of 4H-SiC (347 GPa), γ is surface tension (6.5 J/m² Otubo et al., 2013) and a is the interplanar spacing (3.079 Å) in 4H-SiC.

Substitution of the above values reveals the magnitude of cleavage strength to be 13.53 GPa. Fig. 5 shows the evolution of the tensile stress and shear stress underneath the indenter (the figure was drawn using Eqs. (2)–(6) and (7)) and highlights the theoretical shear strength and theoretical cleavage strength of 4H-SiC.

It can be seen from Fig. 5 and from the above calculations that the theoretical shear strength calculation coincides with the pop-in event observed at an indentation depth of 33 nm whereas the tensile stresses at this point were far lower (10.155 GPa). This proves that the plastic deformation in 4H-SiC during the pop-in event leads to elastic-plastic transition and thus explains that the observed incipient plasticity is due to plastic deformation rather than the micro cleavage or fracture in 4H-SiC. The analysis presented above also reveals that during contact loading of single crystal 4H-SiC, tensile and shear stresses underneath the indenter, increase with an increase in the indentation depth. At shallow depths of indentation (lower than 33 nm while using an indenter with the edge radius of 300 nm), the induced shear stress is lower than the theoretical shear strength of the specimen and hence material showed pure elastic response. With an increase in the extent of displacement, when the shear stress underneath the indenter exceeds the theoretical shear strength of 4H-SiC, a pop-in event is observed, which indicates induced plastic response. Such a plastic response is due to the plastic deformation and not because of the crack propagation because until this point, the theoretical cleavage

strength is much higher than the tensile stress underneath the indenter.

4. Conclusions

Displacement controlled quasistatic nanoindentations on single crystal 4H-SiC were analyzed. Typically below a shear stress of 21 GPa, 4H-SiC showed purely elastic response while plasticity was observed beyond this point. Based on the foregoing discussions, following other conclusions can be drawn:

1. Three distinct patterns in the P - h plots were observed during nanoindentation of 4H-SiC (i) with negative depth hysteresis (ii) with no depth hysteresis and (iii) with positive depth hysteresis. This depth hysteresis is proposed to arise from compressive residual stresses (~ 143 MPa).
2. An analytical stress analysis was carried out to calculate the theoretical shear strength and cleavage strength of 4H-SiC along with the shear stress and tensile stress underneath the indenter. The theoretical shear strength was estimated to be about 20.9 GPa which was found to corroborate with the shear stress (21 GPa) underneath the indenter whereas the theoretical cleavage strength was estimated to be 13.53 GPa which was noted to be much higher than the estimated tensile stress of 10.155 GPa underneath the indenter. Comparison of these values reveals that pop-in event occurred on account of plastic deformation in 4H-SiC rather than fracture (thus indicating that the pop-in event is an outcome of the incipient plasticity in 4H-SiC).

Acknowledgements

Authors greatly acknowledge the funding support from J M Lessells travel scholarship from the Royal Society of Edinburgh (2013 RSE/J M Lessells Travel Scholarship) and an additional funding from the International Research Fellowship account of Queen's University, Belfast. Authors also greatly acknowledge an additional funding from an EPSRC research grant (Ref: EP/K018345/1).

REFERENCES

- Bhattacharya, B., Patten, J.A., and Jacob, J., Single point diamond turning of CVD coated silicon carbide. ASME Conference Proceedings, 2006. 2006(47624): p. 1153-1158.
- Buzio, R., Boragno, C., Biscarini, F., De Mongeot, F.B., Valbusa, U., 2003. The contact mechanics of fractal surfaces. *Nat. Mater.* 2 (4), 233–236.
- Chen, X., Hutchinson, J.W., Evans, A.G., 2005. The mechanics of indentation induced lateral cracking. *J. Am. Ceram. Soc.* 88 (5), 1233–1238.
- Coletti, C., Jaroszeski, M., Hoff, A.M., Sadow, S.E., 2006. Culture of mammalian cells on single crystal SiC substrates. in *Material Research Society Symposium Proceedings*. Cambridge University Press.
- Chrobak, D., Kwang-Ho, Kim., Kurzydowski, K.J., Nowak, R., 2013. Nanoindentation experiments with different loading rate

- distinguish the mechanism of incipient plasticity. *Appl. Phys. Lett.* 103, 072101. <http://dx.doi.org/10.1063/1.4818260>.
- Coletti, C., Jaroszeski, M., Pallaoro, A., Hoff, A., Iannotta, S., Sadow, S., 2007. Biocompatibility and wettability of crystalline SiC and Si surfaces. In: Proceedings of 29th Annual International Conference of the IEEE, Engineering in Medicine and Biology Society. EMBS 2007.
- Demenet, J.-L., Amer, M., Tromas, C., Eyidi, D., Rabier, J., 2013. Dislocations in 4H- and 3C-SiC single crystals in the brittle regime. *Phys. Status Solidi C* 10 (1), 64–67.
- Dharma Raju, T., Kato, M., Nakasa, K., 2003. Backward deviation and depth recovery of load–displacement curves of amorphous SiC film under repeating nanoindentation. *Acta Mater.* 51 (12), 3585–3595.
- Dzurak, A., 2011. Quantum computing: diamond and silicon converge. *Nature* 479 (7371), 47–48.
- Faisal, N., Ahmed, R., Reuben, R., 2011. Indentation testing and its acoustic emission response: applications and emerging trends. *Int. Mater. Rev.* 56 (2), 98–142.
- Faisal, N.H., Ahmed, R., Fu, Y.Q., Elakwah, Y.O., Alhoshan, M., 2012. Influence of indenter shape on DLC film failure during multiple load cycle nanoindentation. *Mater. Sci. Technol.* 28 (9–10), 1186–1197.
- Feldman, D., Parker Jr., J.H., Choyke, W., Patrick, L., 1968. Phonon dispersion curves by Raman scattering in SiC, polytypes 3C, 4H, 6H, 15R, and 21R. *Phys. Rev.* 173 (3), 787.
- Goel, S., Luo, X., Comley, P., Reuben, R.L., Cox, A., 2013. Brittle–ductile transition during diamond turning of single crystal silicon carbide. *Int. J. Mach. Tools Manuf.* 65, 15–21.
- Gouldstone, A., Koh, H.J., Zeng, K.Y., Giannakopoulos, A.E., Suresh, S., 2000. Discrete and continuous deformation during nanoindentation of thin films. *Acta Mater.* 48 (9), 2277–2295.
- Inasaki, I., 1987. Grinding of hard and brittle materials. *CIRP Annal. – Manuf. Technol.* 36 (2), 463–471.
- Javvaji, R., 2008. Nanoscale Ductile Mode Ultraprecision Cutting of Potassium Dihydrogen Phosphate in Mechanical Engineering. National University of Singapore, Singapore.
- Kalnins, U., Erglis, A., Dinne, I., Kumsars, I., Jegere, S., 2002. Clinical outcomes of silicon carbide coated stents in patients with coronary artery disease. *Med. Sci. Monit.: Int. Med. J. Exp. Clin. Res.* 8 (2), P116–P120.
- Komanduri, R., 1996. On material removal mechanisms in finishing of advanced ceramics and glasses. *CIRP Annal. — Manuf. Technol.* 45 (1), 509–514.
- Kruzic, J.J., Kim, D.K., Koester, K.J., Ritchie, R.O., 2009. Indentation techniques for evaluating the fracture toughness of biomaterials and hard tissues. *J. the Mech. Behav. Biomed. Mater.* 2 (4), 384–395.
- Levitas, V.I., Ma, Y., Selvi, E., Wu, J., Patten, J.A., 2012. High-density amorphous phase of silicon carbide obtained under large plastic shear and high pressure. *Phys. Rev. B* 85 (5), 054114.
- Li, X., Wang, X., Bondokov, R., Morris, J., An, Y.H., Sudarshan, T.S., 2005. Micro/nanoscale mechanical and tribological characterization of SiC for orthopedic applications. *J. Biomed. Mater. Res. Part B: Appl. Biomater.* 72B (2), 353–361.
- Luo, X., Goel, S., Reuben, R.L., 2012. A quantitative assessment of nanometric machinability of major polytypes of single crystal silicon carbide. *J. Eur. Ceram. Soc.* 32 (12), 3423–3434.
- Neudeck, P.G., Technology, SiC, 2000. In: Raton, B. (Ed.), *The VLSI Handbook*. CRC Press and IEEE Press, Florida, pp. 6.1–6.24.
- Newsome, D.A., Sengupta, D., Foroutan, H., Russo, M.F., van Duin, A.C., 2012. Oxidation of silicon carbide by O₂ and H₂O: a ReaxFF reactive molecular dynamics study, part I. *J. Phys. Chem. C* 116 (30), 16111–16121.
- Niihara, K., 1979. Slip systems and plastic deformation of silicon carbide single crystals at high temperatures. *J. Less Common Met.* 65 (1), 155–166.
- Otubo, H., Yamamoto, Y., Takekuni, H., Nishitani, S.R., 2013. First Principles Calculations of Relaxed and Reconstructed Surfaces of SiC. Accessed Through google.com on 26.8.2013.
- Patten, J., Gao, W., Yasuto, K., 2005. Ductile regime nanomachining of single-crystal silicon carbide. *J. Manuf. Sci. Eng.* 127 (3), 522–532.
- Patten, J.A., Jacob, J., Bhattacharya, B., Grevstad, Andrew, Fang, Ning, Marsh, E.R., 2007. Numerical simulations and cutting experiments on single point diamond machining of semiconductors and ceramics. In: Yan, J., Patten, J.A. (Eds.), *Semiconductor Machining at the Micro-Nano Scale*. Transworld Research Network, Trivandrum-695 023, Kerala, India (Chapter 2).
- Probe Selection Guide — Hysitron Triboindenter Manual, Incorporated, H., Ed., 2007. Minneapolis, USA.
- Perrone, D., 2007. Process and characterisation techniques on 4H-Silicon Carbide, in *Micronanotechnology* (Ph.D. thesis). Politecnico di Torino, Torino.
- Ravindra, D., 2011. Ductile mode material removal of ceramics and semiconductors, in Department of Mechanical and Aeronautical Engineering. Western Michigan University, Michigan 312.
- Ravindra, D., Patten, J.A., 2007. Determining the ductile to brittle transition (DBT) of a single-crystal 4H-SiC wafer by performing nanometric cutting. In: Proceedings of ISAAT 2007 Precision Grinding and Abrasive Technology at SME International Grinding Conference.
- Ravindra, D., Patten, J., Jacobsen, R., 2013. Hybrid laser ablation–single point diamond turning machining process for CVD–silicon carbide ceramics. *Int. J. Manuf. Res.* 8 (3), 227–249.
- Schuh, C.A., 2006. Nanoindentation studies of materials. *Mater. Today* 9 (5), 32–40.
- Schuh, C.A., Lund, A.C., 2004. Application of nucleation theory to the rate dependence of incipient plasticity during nanoindentation. *J. Mater. Res.* 19 (07), 2152–2158.
- Shayan, A.R., Poyraz, H.B., Ravindra, D., Ghantasala, M., Patten, J. A., 2009. Force analysis, mechanical energy and laser heating evaluation of scratch tests on silicon carbide (4H-SiC) in micro-laser assisted machining ([micro sign]-LAM) process. *ASME Conference Proc.* 2009 (43611), 827–832.
- Shore, P., Cunningham, C., DeBra, D., Evans, C., Hough, J., Gilmozzi, R., Kunzmann, H., Morantz, P., Tonnellier, X., 2010. Precision engineering for astronomy and gravity science. *CIRP Annal. — Manuf. Technol.* 59 (2), 694–716.
- Venkatesh, V.C., Izman, Sudin, 2007. Precision Engineering. Tata Macgraw Hill, New Delhi, India <http://dx.doi.org/10.1036/0071548270>.
- Yan, J., Zhang, Z., Kuriyagawa, T., 2009. Mechanism for material removal in diamond turning of reaction-bonded silicon carbide. *Int. J. Mach. Tools Manuf.* 49 (5), 366–374.
- Zhao, X., Langford, R.M., Shapiro, I.P., Xiao, P., 2011. Onset plastic deformation and cracking behavior of silicon carbide under contact load at room temperature. *J. Am. Ceram. Soc.* 94 (10), 3509–3514.